Journal of Power Sources 190 (2009) 423–434

Contents lists available at ScienceDirect

Journal of Power Sources

journal homepage: www.elsevier.com/locate/jpowsour

Highly porous PEM fuel cell cathodes based on low density carbon aerogels as Pt-support: Experimental study of the mass-transport losses

Julien Marie[a,*], Regis Chenitz[a], Marian Chatenet[b], Sandrine Berthon-Fabry[a], Nathalie Cornet[c], Patrick Achard[a]

[a] Centre d'Energétique et Procédés, Ecole des Mines de Paris, Rue Claude Daunesse, 06904 Sophia-Antipolis, France
[b] Laboratoire d'Electrochimie et de Physicochimie des Matériaux et des Interfaces, UMR 5631 CNRS/INPG/UJF, 1130 rue de la piscine, 38402 Saint Martin d'Hères Cedex, France
[c] Renault, Direction de l'Ingénierie des Matériaux, 1 avenue du Golf, 78280 Guyancourt, France

ARTICLE INFO

Article history:
Received 7 September 2008
Received in revised form 8 January 2009
Accepted 18 January 2009
Available online 17 March 2009

Keywords:
PEM fuel cells
Carbon aerogels
Cathode
Catalyst
Platinum
Transport losses

ABSTRACT

Carbon aerogels exhibiting high porous volumes and high surface areas, differentiated by their pore-size distributions were used as Pt-supports in the cathode catalytic layer of H_2/air-fed PEM fuel cell. The cathodes were tested as 50 cm^2 membrane electrode assemblies (MEAs). The porous structure of the synthesized catalytic layers was impacted by the nanostructure of the Pt-doped carbon aerogels (Pt/CAs). In this paper thus we present an experimental study aiming at establishing links between the porous structure of the cathode catalytic layers and the MEAs performances. For that purpose, the polarization curves of the MEAs were decomposed in 3 contributions: the kinetic loss, the ohmic loss and the mass-transport loss. We showed that the MEAs made with the different carbon aerogels had similar kinetic activities (low current density performance) but very different mass-transport voltage losses. It was found that the higher the pore-size of the initial carbon aerogel, the higher the mass-transport voltage losses. Supported by our porosimetry (N_2-adsorption and Hg-porosimetry) measurement, we interpret this apparent contradiction as the consequence of the more important Nafion penetration into the carbon aeorogel with larger pore-size. Indeed, the catalytic layers made from the larger pore-size carbon aerogel had lower porosities. We thus show in this work that carbon aerogels are materials with tailored nanostructured structure which can be used as model materials for experimentally testing the optimization of the PEM fuel cell catalytic layers.

1. Introduction

Achieving PEM fuel cell air-fed cathodes with optimal performances requires dispersing the total amount of electrocatalyst on a high surface-area support, while preserving reactants and products access to the catalytic sites. Although high surface-area carbon blacks yield appropriate platinum particles dispersion over the substrate, their use can lower fuel cell performance [1]. Indeed, high surface-area carbon blacks (over 500 $m^2\,g^{-1}$) are constituted of small primary carbon particles (10–15 nm) covalently linked as aggregates which agglomerate by soft bonds (Van der Waals) yielding small pores and these small pores can hinder transport mechanisms to the Pt particles.

State-of-the-art catalysts made from Pt supported on high surface area carbon blacks cope with this problem thanks to their high loadings in platinum (50 wt.% Pt and more). For a given Pt loading of the electrode ($mg_{Pt}\,cm^{-2}$), this enables to make thinner catalytic layers with low mass-transport potential losses despite their low porosity. Nevertheless, as mentioned by Gasteiger et al. [2], a further reduction of these losses is one of the requirements to further improve the performances and reach marketable PEMFC. In this way, our work focuses on a relatively recent type of porous carbon, called carbon aerogels [3], because carbon aerogels could be relevant to overcome this issue.

The similarity between carbon aerogels and carbon blacks is that they can be both made of small primary carbon particles, the size of which determines their surface area (over 500 $m^2\,g^{-1}$ for carbon particles of diameter typically around 10 nm). The major difference between carbon blacks and carbon aerogels is the arrangement of these primary carbon particles, i.e. their porous structure. For carbon aerogel, this arrangement can be tuned without changing significantly the size of the particles by the sol–gel synthesis parameters (reactants concentration in the sol and precursors ratio). Therefore surface area and porous properties (pore size and porous volume) of carbon aerogels are not linked. Whereas, in the case of carbon blacks, the porous properties are determined by the carbon particle aggregates structure and agglomeration of these aggregates which are hardly controllable and makes that the size of

* Corresponding author. Tel.: +33 679992062; fax: +33 148395878.
E-mail address: julien.marie@saint-gobain.com (J. Marie).

0378-7753/$ – see front matter © 2009 Elsevier B.V. All rights reserved.
doi:10.1016/j.jpowsour.2009.01.047

the carbon particle (i.e. surface area) and volume properties are linked.

The carbon aerogels used in this study have relatively large pore-size and high porous volumes (>90% porosities) with high surface area. Such a combination of properties is not achievable with carbon blacks. This makes carbon aerogels interesting for both improving performances and studying mass-transport losses of the PEMFC cathode.

Carbon aerogels, which can be seen as a volume of space tridimensionally delimited by a thin carbon skeleton, have already successfully been used as heterogeneous catalyst supports. Gas phase catalytic reactions have been improved by the high porosity of carbon aerogels, which facilitates the reactant diffusion to the catalytic sites [4].

In this work, the mass-transport voltage losses of PEMFC cathodes, already studied by several groups [2,5,6], have been extracted from experimental polarization curves ($U = f(i)$). These losses are usually associated with the diffusion of oxygen through the electrode structure (i.e. pores and Nafion films covering the catalyst particles). Proton transport into the perfluorinated ionomer network [6] may also contribute to these losses, as this conduction mechanism may not only have an ohmic contribution. Indeed, proton conduction in Nafion is a complex mechanism. It is interpreted by Tsampas et al. [7,8] both as proton bulk-migration in the water domains of the membrane and as proton surface-migration by tunneling at the surface of the ionic domains. Finally, the mass-transport losses are also impacted by the water produced by the oxygen reduction reaction (ORR) at the catalytic sites and carried by humidified reactant gases.

Most importantly, the design of the catalytic layer requires to understand the dependence of the mass-transport mechanisms with the catalytic layer nanostructure. So this preliminary work initiates the experimental study of the mass-transport losses in PEMFC cathodes by using a tunable porous carbon support, namely carbon aerogels.

We synthesized Pt-doped carbon aerogels [9–11] to elaborate porous cathode catalytic layers. Then, we assembled these catalytic layers in membrane electrode assemblies (MEAs) and measured their: (i) active platinum surface area, (ii) carbon double-layer capacitance and (iii) performance when fed with air on a single-cell testing bench.

In our previous work [9] rotating disk electrode (RDE) measurements showed that platinum nanoparticles with identical dispersion and ORR kinetic activities could be deposited on two carbon aerogels having different porous structures with fixed Pt properties, enabling to study the effect of the carbon aerogel structure.

We also performed the electrochemical characterization in half-cell configuration of catalytic layers [10] made with Pt-doped carbon aerogels on small (0.75 cm^2) electrodes immersed in 1 M sulfuric acid solution. This work showed that the structure of the carbon aerogel has a major influence on the structure of the catalytic layer.

Following those results, the present paper aims at establishing links between the structure of the cathodes made from carbon aerogel-supported platinum nanoparticles (Pt/CA) with their electrochemical performance in MEA configuration. Our experimental work lies on the comparison of: (i) two carbon aerogels CA#1 and CA#2, exhibiting different porous structures and (ii) various catalytic layers realization techniques.

Table 1
Carbon, platinum and Nafion loadings, L_C, L_{Pt}, L_N of the cathode catalytic layers (50 cm^2) of the "Ink" MEAs, "Reference-0.6" MEA prepared for fuel cell characterization. "Nafionless" and "S" MEAs prepared for the evaluation of the cathode realization technique.

	L_C ($mg_C\ cm^{-2}$) (±10%)	L_{Pt} ($mg_{Pt}\ cm^{-2}$) (±10%)	L_N ($mg_N\ cm^{-2}$) (±10%)
CA#1-I-0.5	1	0.5	0.5
CA#1-I-0.21	0.42	0.21	0.21
CA#2-I-0.5	1	0.5	0.5
CA#2-I-0.21	0.42	0.21	0.21
CA#2-I-0.13	1	0.13	0.5
Reference-0.6	0.9	0.6	0.33
CA#1-S-0.28	0.56	0.28	0.28
CA#2-S-0.08	0.16	0.08	0.08
CA#2-0.1	0.2	0.1	0.1

2. Experimental

2.1. Preparation of the MEAs with carbon aerogel-based cathode catalytic layers using an ink technique

The synthesis parameters of the carbon aerogels used in this work (CA#1 and CA#2) and the Pt insertion technique are described in our previous studies [9,11]. The Pt loading obtained on both carbon aerogels was 33.7 ± 0.1 wt.%. These catalysts were obtained as powders consisting of micron-sized carbon aerogel grains resulting from the crushing of the initially cm-sized carbon aerogel monoliths in an agate mortar, operation which does not destroy the initial mesoporosity of the carbon aerogel. To make the inks, the Pt/CAs were suspended as a powder into a low concentration (0.3 wt.%) [12] aqueous suspensions of Nafion by using a commercial 10 wt.% Nafion suspension in water (Ion Power Inc. DE1020). The inks were magnetically stirred for 24 h and then sonicated for 1 min with an ultrasonic generator before being sprayed to make the cathode catalytic layers.

The spray was applied onto a Kapton foil in front of which was placed another Kapton foil with a 7.1 cm × 7.1 cm slot. These foils (75 μm thickness each) were placed on a heating plate to keep the sprayed surface at about 100 °C, so that the water of the ink evaporated continuously while spraying. The subsequent assembly of the catalytic layer on the Nafion membrane was realized by hot-pressing (20 MPa, 120 °C, 2 min) the Kapton decal against a Nafion NE1035 membrane (DuPont membrane, purchased from IonPower Corp.). The membranes and the Kapton foils were washed beforehand in boiling HNO_3 0.5 M for 1 h and rinsed in boiling deionized water bath for at least 1 h.

A commercial catalyzed carbon felt was used as the anode in all the MEAs tested. The catalyst (4 wt.% Pt-doped carbon black from TKK) was deposited by the Paxitech company onto the carbon felt (GDL 2315 I6 with PTFE treatment, from Freudenberg GmbH) with 0.6 $mg_{Pt}\ cm^{-2}$ platinum loading mixed with Nafion 0.24 $mg_N\ cm^{-2}$ (i.e. N/C = 0.36). The same carbon felt was used as the cathode GDLs. The cell gaskets (adapted to the GDL from Freudenberg) were finally placed on the membrane. This constituted the assembly which was hot-pressed at 3 bar, 70 °C (to ensure better handling and contact at the cathode GDL–catalytic layer interface) before being placed between graphite flow-fields plates. The cell end plates where tightened by 10 screws on which 3 N m angular momentum was applied.

The 50 cm^2 cathode catalytic layers of the MEA all had the same Nafion/Carbon (N/C) ratio of 0.5. The main adjustable parameter for the preparation of the MEAs was the platinum loading of the cathodes, so the MEAs are referenced as follows. The CA#1-I-0.5 MEA has a cathode catalytic layer prepared from the Pt-doped carbon aerogel CA#1 and the cathode platinum surface loading is 0.5 $mg_{Pt}\ cm^{-2}$. The letter "I" signifies that an ink technique (described below) has been used to make the catalytic layer. Table 1 summarizes the MEA properties that will be presented hereafter.

In order to characterize the commercial (Paxitech company) catalyzed felt which was used as anodes in all the aforementioned MEAs and to validate our measurement technique, a reference MEA was made from the assembly of two of these Paxitech electrodes,

hot-pressed against the Nafion membrane NE1035. This MEA is called Reference-0.6 referring to its cathode Pt loading.

The ink technique described (MEA labeled "I") above is one of the most employed technique found in the literature (similar to the so-called thin-film technique [13,14]) using carbon blacks as platinum-support. So because carbon aerogel is a new catalyst support which has major structural differences with carbon blacks, we wanted to determine if the ink technique employed to disperse the Nafion polymer on the carbon surface was efficient. For that purpose, two other different preparation techniques were employed to make the Pt-doped carbon aerogel cathodes.

The first variation of our standard ink technique was the "Nafion-less" technique consisting in spraying a Pt-doped carbon aerogel water suspension (without any Nafion) on the Kapton decal and pressing it against the Nafion membrane. By testing this kind of catalytic layer (CA#2-0.1), we intended to measure whether the hot-pressing of the catalytic layer against the membrane could yield a significant penetration of the Nafion inside the catalytic layer. The second variation of the cathode realization technique (MEA labeled "S") consisted of spraying the Nafion colloidal suspension (0.3 wt.%, same as in the inks) on the top of the Pt/CA layer which were sprayed beforehand.

2.2. Characterization of the materials

2.2.1. Intrinsic platinum deposit properties

The intrinsic properties of platinum on the carbon aerogels were obtained (rotating disc electrodes experiments) in our previous study [9]. We showed that platinum deposited on CA#1 and CA#2 exhibited similar electrochemically active Pt-surface area ($S_{Pt} = 43 \pm 2\ m^2 g_{Pt}^{-1}$) and ORR activities in O_2 saturated H_2SO_4 (1 M) solution at room temperature ($i_m = 9 \pm 0.1\ A\ g_{Pt}^{-1}$ at 0.9 V vs. NHE).

2.2.2. Porous structure characterization

For the measurement of the porosity of the Pt/CA + Nafion layers, only the cathode catalytic layer was deposited on one side of the Nafion membrane. These catalyzed membranes were cut in stripes fitting inside the porosimeter chamber (1–2 cm). For this particular characterization, two different Nafion loadings were tested (25 and 40 wt.%) and the loadings in Pt/CAs were $0.1 \pm 0.01\ mg\ cm^{-2}$. The combination of N_2-sorption and Hg-porosimetry techniques was required to characterize the porosity of the layers made with carbon aerogels because their pore-sizes extend in the domain of large mesopores (around 50 nm). N_2-sorption isotherms precisely yield the BET surface area (S_{BET}) and the microporous volume (V_{mic}) whereas the mesoporous volume is underestimated if only N_2-sorption is used [15] so it was mainly measured from Hg-porosimetry which is a direct measure of the porous volume. So we used the Hg-porosimeter to its maximum pressure (2000 bar) to measure the porous volume of all the pores larger than 7.5 nm whereas the remaining small mesopores (between 2 and 7.5 nm) porous volume ($V_{mes}(2–7.5\ nm)$) was assessed from the N_2-sorption isotherms. The total porous volume was thus obtained from the following equation:

$$V_p = V_{mic} + V_{mes}(2 - 7.5\ nm) + V_{Hg} \quad (1)$$

The pore-size distributions derived from Hg-porosimetry were calculated from an adapted hierarchical pore collapse theory introduced by Pirard et al. [16]. Indeed using the commonly used Washburn equation yields a false result in terms of pore size because it does not account for the deformation of the porous structure occurring before the intrusion of Hg. In fact, the intrusion of mercury occurred only at high Hg pressure so that the majority of the pore sizes were assessed from the Pirard et al model as presented in [10].

2.2.3. Porous structure observation

The relative complexity of the interpretation of the measurements of highly porous carbon aerogel structure to draw pore-size distributions rendered necessary the direct observation by scanning electron microscope (SEM) of the carbon aerogels porosity and of the Nafion insertion in their structure. This was done by means of a SEM equipped with a field emission gun detector (FEG-SEM).

2.2.4. Catalytic layers activity measurement, 50 cm^2 MEA configuration

2.2.4.1. Operation of the testing bench. The 50 cm^2 MEAs electrochemical properties were measured on a single-cell testing bench designed and assembled in our laboratory. The MEA was fed with H_2/air (H_2 Air Liquide alphagaz 2). Oxygen (O_2 Air Liquide alphagaz 2) was also used in comparison with air at the cathode, as presented in Section 3.6.2.2. The total pressure (P_{tot}) of the gases was controlled by pressure regulators (Bronkhorst) placed upstream of the gas line exhaust. The gas flow rates were controlled by means of mass flow regulators (Bronkhorst) which were placed at the input of the gas line circuit, upstream to the gas humidifiers (controlled evaporator mixers from Bronkhorst). The humidifiers enabled to tune the relative humidity by controlling the mass flow rate of input water. For this study, only 100% relative humidity was used. The cell inlet pipes and the controlled evaporator mixers were overheated of 5 °C over the cell temperature (70 °C), preventing water condensation before the cell. The cell temperature was controlled by heating cartridges placed inside the cell stainless steel holding plates. The cartridges power output was regulated using a thermocouple placed 1 cm inside the cell cathode graphite flow plate. The gas temperature was recorded at several points along the flow-fields at the anode and cathode side.

The cell voltage was controlled by means of a numeric high power potentiostat (Biologic HCP-803, 80 A—3 V, 240 W). Each new MEA was submitted to a start-up procedure consisting of keeping the cell between 0.4 and 0.5 V for half a day with short periods at 0.8 V. The MEA performance improved during this start-up procedure and stabilized at the end of it. The experimental data points of the polarization curves were measured at the stabilization of the intensity about 15 min after setting the cell voltage. This procedure enabled to obtain ongoing and backward points close to each other.

2.2.4.2. Platinum surface area and capacitance measurement. The electrochemical platinum surface area (ECSA) and carbon double-layer capacitance of the cathodes were obtained from cyclic voltammograms recorded between 0.05 and 1 V vs. NHE in the single cell testing bench. For this measurement, the cathode, fed with humidified nitrogen, was the working electrode (WE). The anode was fed with humidified hydrogen and was taken as the reference electrode (RE) and the counter electrode (CE) at the same time. Considering the anode as a reference electrode and as the counter electrode at the same time could be a problem since its potential may change with the current. But the hydrogen oxidation is very reversible and the currents are of small intensity, so we can consider that the potential of the anode is constant, as well-documented in the literature under the dynamic hydrogen electrode appellation [17,18].

The voltammograms obtained on the Reference-0.6 MEA compared with a typical MEA CA#1-I-05 are shown in Fig. 1.

The ECSA was measured from the coulometry of the H-adsorption–desorption peaks [11], which corresponds to the dashed and grey domains on the cyclic voltammograms of Fig. 1. The carbon double-layer capacitance was calculated from the voltammograms in the potential domain 0.35–0.45 V where the platinum yields no specific current and no faradic reaction occurs [19]. The current measured in this potential domain (double-layer current i_{dl}) is linked to the carbon double-layer capacitance C_{dl}^{total} by the

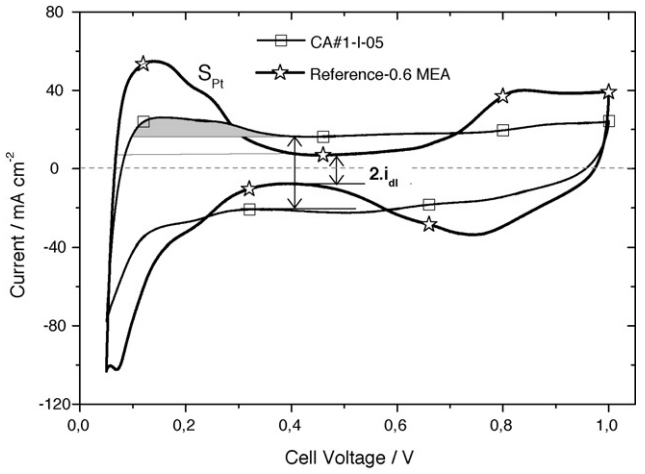

Fig. 1. Cyclic voltammograms. Reference-0.6 MEA, compared with a carbon aerogel containing MEA CA#1-I-05. Cathode (WE) under N_2, potential sweep rate (dU/dt) = 0.1 V s^{-1}, 70 °C, anode (CE = REF) under H_2.

following equation:

$$i_{dl} = C_{dl}^{total} \frac{dU}{dt} \quad (2)$$

with dU/dt the potential sweep rate.

As stated above, we assumed constant potential at the hydrogen electrode during the measurement, which implies that the Faradic current at the negative electrode (PEMFC anode) is potentially orders of magnitude higher than that of the positive electrode (PEMFC cathode). Therefore, the measured current must be limited by the capacitive current provided at the cathode, due to double-layer phenomena. Consequently, the carbon double-layer capacitance measured in such experiment is only relative to the cathode, and the carbon/Nafion contact at the hydrogen electrode does not contribute to the total capacitance. According to Eq. (3), this implies that the anode capacitance under hydrogen is infinite (in fact, this infinite value translates the fast hydrogen oxidation/evolution reaction):

$$\frac{1}{C_{dl}^{total}} = \frac{1}{C_{dl}^{anode}} + \frac{1}{C_{dl}^{cathode}} \approx \frac{1}{C_{dl}^{cathode}} \quad (3)$$

As no signal, neither from carbon nor from the platinum contained in the cathode, can be recorded in the lack of ionic contact by the Nafion ionomer [20], the measurement of the Pt surface area and the double-layer capacitance give an indication of the penetration of the Nafion into the porous structure of the positive electrode (PEMFC cathode) catalytic layers based on carbon aerogels.

2.2.4.3. Ohmic resistance measurement. The ohmic resistances of the MEAs, measured on the single-cell testing bench, were taken as the value of the complex impedance Z of the cell when $\mathrm{Im}(Z) = 0$ at high frequency [21]. We controlled the potentiostat so that it applied to the cathode (fed with 100% R_H nitrogen) a potential perturbation of 20 mV over a fixed cell potential (open circuit, 0.8 or 0.4 V) at 32 different frequencies between 0.1 Hz and 0.2 MHz.

This way of measuring the ohmic resistance was reproducible and precise but unfortunately it does not comprise all the contribution to the ohmic resistance of the MEA. According to Makharia et al. [22], the most considerable part of the resistance that is not measured at high frequency is the ionic resistance of the cathode catalytic layer.

In situ determining the ionic conductivity of the PEMFC cathode catalytic layer (during operation), requires theoretical considerations and modeling of the catalytic layer [5,22]. As this preliminary

Table 2
Comparison of the porous volumes measured between 2 and 50 nm from N_2-sorption, the total porous volume, pore-size distribution (PSD) peak position and PSD min–max for the two carbon aerogels CA#1 and CA#2 and the active layers made using two different Nafion loadings 25 and 40 wt.%. The values are related to the total mass of the layers excepted S_{BET} and V_{mic}. The Pt loading for all the layers = 0.1 ± 0.01 mg cm^{-2}.

	ρ_b (g cm^{-3}) ±10%	S_{BET}[a] (m^2 g_c^{-1}) ±10%	V_{mic} (<2 nm)[a] (cm^3 g_c^{-1}) ±10%	V_{mes} (2–7.5 nm) (cm^3 g^{-1}) ±10%	V_{mes} (2–50 nm) (cm^3 g^{-1}) ±10%	V_{Hg} (>7.5 nm) (cm^3 g^{-1}) ±10%	V_p (cm^3 g^{-1}) ±10%	PSD peak (nm)	PSD min–max (nm)
CA#1	0.15	669	0.33	0.12	1.79	5.15	5.6	38	10–70
CA#2	0.19	565	0.26	0.09	1.93	4.45	4.8	25	10–50
CA#1-N25	–	183	0.08	0.098	0.85	0.75	0.90	15	10–25
CA#1-N40	–	281	0.11	0.095	0.55	0.4	0.55	15	10–25
CA#2-N25	–	453	0.21	0.12	1.75	2.2	2.96	20	10–50
CA#2-N40	–	356	0.14	0.1	0.78	0.8	1.47	20	10–30

[a] Values related to the mass of carbon only.

work is based on experimentation, it seemed reasonable to assimilate the unmeasured part of the ionic conductivity as a mass-transport loss.

3. Results and discussion

3.1. Porosity of the Pt-doped carbon aerogel/Nafion-based catalytic layers

We will recall in this part the results of the porosity characterizations from our previous studies [9,10]. The surface area, porous volumes and pore-size distributions (PSD) are described in Table 2. The PSD are described by the position of their peak (PSD maximum value position) as well as the minimum and maximum value of pore-size of the distributions.

Table 2 shows that CA#1 and CA#2 catalytic layers exhibit very different porosities. It is found that, the higher the initial carbon aerogel pore-sizes (CA#1), the lower the porosity of the layers made from it. This must result from the more important Nafion insertion in the larger pores of CA#1. This carbon aerogel must be better wetted by Nafion in the ink and then much more intruded during the hot-pressing step. Notice that even the lowest porous volume recorded on CA#1-N40 layer (0.55 $cm^3\ g^{-1}$) is relatively high compared with the porous volumes measured in carbon black-based catalytic layers [23].

3.2. FEG-SEM observation of the carbon aerogels

Fig. 2 shows FEG-SEM pictures of the interior of carbon aerogel containing layers. They were obtained by peeling-off the carbon felt (used as gas diffusion layer) initially hot pressed against the surface of the layers. The peeling mechanical action reveals the interior of the carbon aerogel layers at some part of their surface. Compared to the observation of cross-sections of the layers, this technique requires no preparation and does not disturb (no blade used) the structure of the layer. The nanostructure of the layers is thus observable. Fig. 2A and B, respectively, shows layers only made from Pt-doped carbon aerogels CA#1 and CA#2. The layers made from Pt-doped carbon aerogels CA#1 and CA#2 with 40 wt.% Nafion are shown in Fig. 2C and D, respectively.

These images firstly show that the primary carbon particle network constituting the CA skeleton is still visible after the hot pressing step at 200 bar, 120 °C against the Nafion membrane. Carbon aerogel micron-sized grains are not destroyed during the elaboration of the MEA. In fact, this feature was predictable from the behavior of the carbon aerogels monolith upon compression by mercury during Hg-porosimetry measurement [10], which exhibited the considerable flexibility of this material: carbon aerogel monoliths undergo a reversible deformation, at least until a Hg pressure of 500 bar. From this prospect, the Pt/CA materials should be less altered during the PEMFC MEA elaboration process than the Pt/carbon blacks. Carbon black grains should thus be more prone to: (i) self-"ball-milling" and (ii) Pt particles detachment, as well documented by the Los-Alamos group [24], because the carbon black agglomerates are not covalently bounded to each other.

On the pictures of Nafion containing layers (Fig. 2C and D), the carbon aerogel particles appear "glued", the primary particles network seems entangled in the Nafion polymer phase. These observations are in line with the important modification of the porous volumes and surface area of the samples after Nafion insertion (Table 2). Nevertheless, the different penetration of Nafion in CA#1 and CA#2 shown by the porosity measurements could not be observed on these FEG-SEM pictures: the comparison of the extent of Nafion penetration is difficult to evaluate. Also notice that the difference between CA#1 and CA#2 in terms of primary particle size and pore size is not clear on these pictures. This is due to: (i) the too small difference between the primary particles size of CA#1 (10 nm) and CA#2 (6–7 nm), only precisely measured by TEM and (ii) the highly interconnected pore structure of the carbon aerogels, which renders difficult any precise determination of

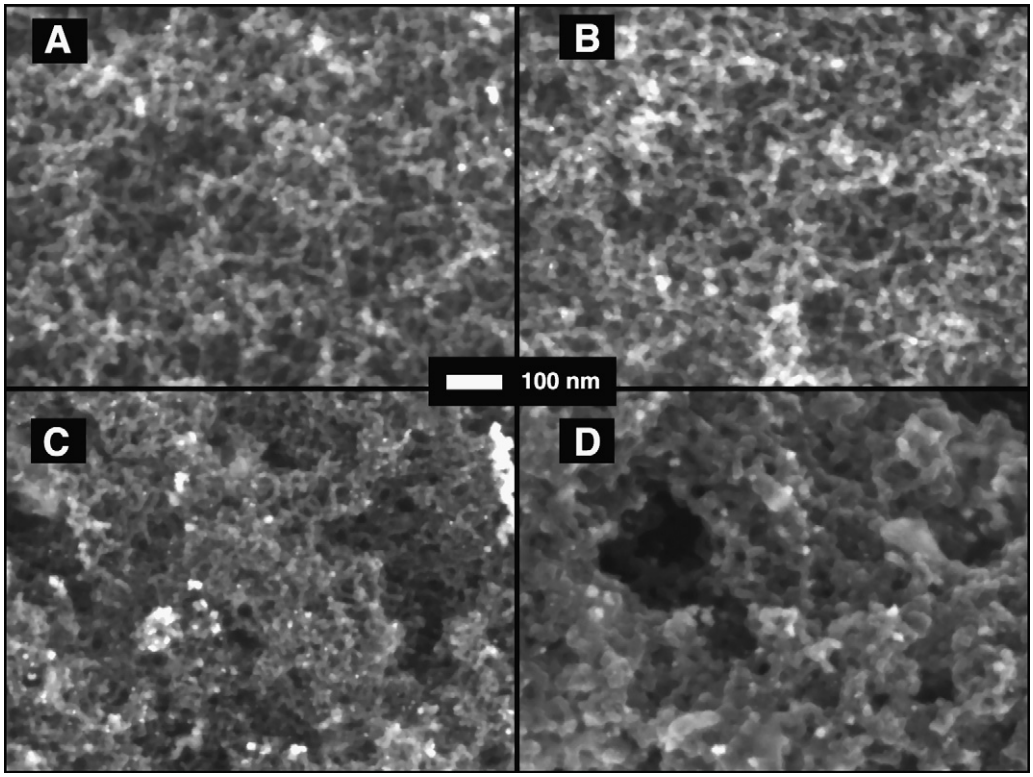

Fig. 2. FEG-SEM observation of carbon aerogel layers: (A) CA#1 only, (C) CA#2 only, (B) CA#1-N40 (i.e. 40 wt.% Nafion) and (D) CA#2-N40.

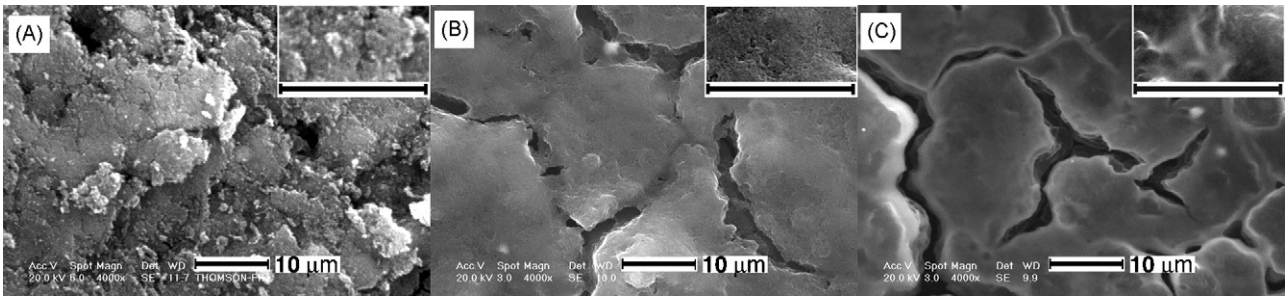

Fig. 3. SEM observation of carbon aerogel (CA#1) catalytic layers: (A) carbon aerogel-only (Nafionless) layer, (B) "I" catalytic layer: ink of carbon aerogel mixed with Nafion sprayed on the Kapton support and (C) "S" catalytic layer: carbon aerogel only layer with a Nafion suspension sprayed over it. Scale bars: 10 μm.

the pore size (even the pore size definition is not trivial in carbon aerogels).

Then we compared by SEM the layers sprayed on the Kapton films before hot pressing against the membrane in order to determine the organization of the grains of carbon aerogel at the micron scale. The layer prepared by the ink technique was compared to a layer with no Nafion (only the Pt/CA water suspension was sprayed) and the same layer with a spray of the diluted (0.3 wt.%) Nafion suspension applied afterwards on the layer.

The SEM observations (Fig. 3) revealed important changes in the aspect of the Pt/CA layers depending on the preparation technique used. The layer with no Nafion (A) has a relatively high rugosity, the unagglomerated micron-sized grains of carbon aerogel are visible. The ink layer (B) exhibits wider domains (grains connected by Nafion). The surface is smoother but still textured showing that Nafion does not fully obstruct the porosity of the carbon aerogels. Contrarily, the Nafion-sprayed catalytic layer (C) seems covered by a smooth film: even at high magnification (inset) the porosity of the carbon aerogel is not visible. This indicates that the sprayed Nafion penetrated less deeply into the carbon aerogel structure than during impregnation in the ink. On account of these observations the ink technique seems to yield a relatively efficient penetration of the Nafion in the catalytic layer and should yield a significant utilization of Pt.

3.3. Active platinum surface area measurement in MEA

To represent the effective penetration of the Nafion in the porous structure of the carbon aerogel-based cathode catalytic layers, we calculated the Pt utilization ratio u_{Pt} defined as:

$$u_{Pt} = \frac{S_{Pt}^{MEA}}{S_{Pt}^{RDE}} \quad (4)$$

with S_{Pt}^{RDE} the ECSA measured in RDE configuration equals to $42 \pm 3\ m^2\ g^{-1}$ on both carbon aerogels [9] and S_{Pt}^{MEA} the ECSA measured in MEA configuration.

First of all, the data in Table 3 shows that no clear distinction can be made between the ECSA of the MEAs made with CA#1 and CA#2. The main differentiation between the results is due to the layers realization technique: cathodes made with the ink technique ("I") have higher ECSA and thus higher Pt utilization ratio. This means that the ink preparation technique, as supposed from the SEM observations, is beneficial for the contact between platinum and Nafion.

Interestingly, we can see when comparing CA#1-I-0.5, CA#1-I-0.21, CA#2-I-0.5 and CA#2-I-0.21 that increasing the platinum loading lowers the ECSA (20% decrease for CA#1 and 40% decrease for CA#2) whereas no dependence should exist. This could be due to the penetration of the Nafion membrane into the thinner layers during the hot-pressing step. Assuming that the penetration of Nafion in the layer in only depending on the pressure and temperature of the hot pressing step and is independent from the layer thickness, a more important fraction of the thinner layers would be impacted by the hot pressing step.

Related to this observation, the non-neglectable ECSA measured on the MEAs CA#1-S-0.28 and CA#1-0.1 indicates that the hot-pressing step enables a relatively deep penetration of the Nafion into the layer, which renders about 20% of the cathode catalytic layer platinum active. It is worth noticing that hydrogen surface diffusion between the platinum nanoparticles and the carbon surface (hydrogen spillover [25]) could also contribute to the overall charge of hydrogen adsorption–desorption during the voltammetry cycles. This mechanism could make Pt particles to contribute to the ECSA even if they were not connected to Nafion. But because surface diffusion is a slow process it is likely negligible in our case (cyclic voltammograms sweep rate = 100 mV s^{-1}).

We finally underline two limitations to our measurement of the ECSA. The first one is the 24 h magnetic stirring that we applied to the inks before their spraying onto the Nafion membrane which is likely lowering the u_{Pt} values [24]. The second one is intrinsic to the technique of hydrogen adsorption–desorption that we used. Its limitations was studied recently by Shinozaki et al. [26] who

Table 3
Characterization of the catalytic layers by cyclic voltammetry in MEA configuration, the Pt utilization ratio is based on a platinum surface area measured in RDE configuration of $42 \pm 3\ m^2\ g^{-1}$, Pt wt.% ratio on both carbon aerogels CA#1 and CA#2 = 33 wt.%.

	L_{Pt} ($mg_{Pt}\ cm^{-2}$) ±10%	S_{pt}($m^2\ g_{pt}^{-1}$) ± 10%	u_{Pt} (%)
CA#1-I-0.5	0.5	17.1	41
CA#1-I-0.21	0.21	20.7	47
CA#2-I-0.5	0.5	15.7	36
CA#2-I-0.21	0.21	26	59
CA#2-I-0.13	0.13	20.6	47
Reference-0.6	0.6	64	73 [2]
CA#1-S-0.28	0.28	9.8	22
CA#2-S-0.08	0.08	3.2	7
CA#2-0.1	0.1	8.5	19

Table 4
Characterization of the catalytic layers by cyclic voltammetry in MEA configuration, cathode catalytic layer capacitance measurement from the carbon double-layer current, utilization of carbon u_c defined in Eq. (5), compared with the platinum utilization u_{Pt}.

	$C_{cathode}$ ($F\ g^{-1}$) ±20%	u_C (%)	u_{Pt} (%)
CA#1-I-0.5	193	58	41
CA#1-I-0.21	181	54	47
CA#2-I-0.5	85	30	36
CA#2-I-0.21	219	78	59
CA#2-I-0.13	154	55	47
Reference-0.6	68	NA	73
CA#1-S-0.28	67	20	22
CA#2-S-0.08	82	29	7
CA#2-0.1	79	28	19

compared several experimental methods to estimate the available and electrochemically active Pt surface area on conventional Pt/C catalysts. They showed that comparing the H-adsorption on Pt (i.e. using H probe) on a rotating disc electrode and in MEA configuration is entangled with experimental problems that we also noticed. For example, the dependence of the H desorption charge with the cyclic voltammogram lower limit and sweep rate. The aforementioned authors demonstrated that Pt surface area measurement based on CO probe is less prone to such measurement error. They observed a 12% under-estimation of Pt utilization when using the H probe compared with the CO probe.

3.4. In situ carbon double-layer capacitance measurement

In addition to the platinum surface area measurements, which evaluated the efficiency of the Nafion impregnation or the eventual electronic insulation of some carbon aerogel grains, a similar evaluation could be made from the "carbon signals" on the cyclic voltammograms, that is, the double-layer current yielding the carbon double-layer capacitance. The same way that Pt is not active when disconnected from Nafion, the double-layer capacitance only arises where Nafion contacts the carbon surface, especially for volumic (gas diffusion) electrodes, by opposition to microscopic electrodes [25].

The specific capacitance values (up to $219\,F\,g^{-1}$) for the various cathodes in Table 4 are relatively high as compared with the literature values ($\sim 100\,F\,g^{-1}$) for carbon aerogels [27]. This overestimation could be due to the existence of pseudo-capacitive currents, originating from the quinone–hydroquinone redox peaks monitored in the range 0.4–0.6 V vs. SHE (i.e. in the same potentials range where double-layer currents are monitored).

To compare these data to the Pt utilization ratio, we considered a surface specific carbon double-layer capacitance of $50\,\mu F\,cm^{-2}$ which is in the high range of the values reported by Kinoshita [19]. This yields a theoretical maximum capacitance by multiplying it by the carbon aerogel surface area: $C_{max}^{theoretical} = 50(\mu F\,cm^{-2}) \times S_{BET}(m^2\,g^{-1})$ giving $C_{max}^{theoretical}(CA\#1) = 334\,F\,g^{-1}$ and $C_{max}^{theoretical}(CA\#2) = 282\,F\,g^{-1}$.

So we translates the experimental double-layer capacitance values as fractions of this theoretically "available" capacitance on the carbon, i.e. by the carbon utilization ratio u_C defined as follows:

$$u_C = \frac{C_{cathode}^{measured}}{C_{max}^{theoretical}} \quad (5)$$

We can notice in Table 4 that u_C and u_{Pt} roughly display the same variations taking into account that the measurement uncertainty of the capacitance is about 20% for several experimental reasons such as non-symmetry of the voltammograms, non-negligible contribution of pseudocapacitive currents. Obtaining an agreement between u_{Pt} and u_C is an indication of the homogeneity of the platinum deposit on the carbon surface.

3.5. Fuel cell testing of the MEAs: polarization curves

As expected from the measurement of the Pt utilization ratio, the performance of the cathodes which were not made by the ink technique, shown in Fig. 4 as the "group 1", are quite poor compared with the ink ("I") MEAs, shown as the "group 2". Thus, in the following parts, our analysis will be based on the "I" layers.

The novelty of the results presented in Fig. 4 consists in the measurement of the major effect of the carbon aerogel porous structure on the cell polarization at high current density. The similarity of the polarization curves at low current density, which will be detailed in Section 3.6.2.2, confirms our previous results in RDE configuration [9]. The differences measured between the MEAs originate in the carbon aerogel nanostructure and not in the Pt deposit. These experimental results undoubtedly show that not only the Pt utilization factor (u_{Pt}) is important (i.e. how much Pt is "wetted" by Nafion), but also the Pt effectiveness factor (ε), representing how this Pt is accessible to reactant, a concept first introduced by Stonehart and Ross [28] later applied to PEMFC cathode by Gloaguen et al. [29].

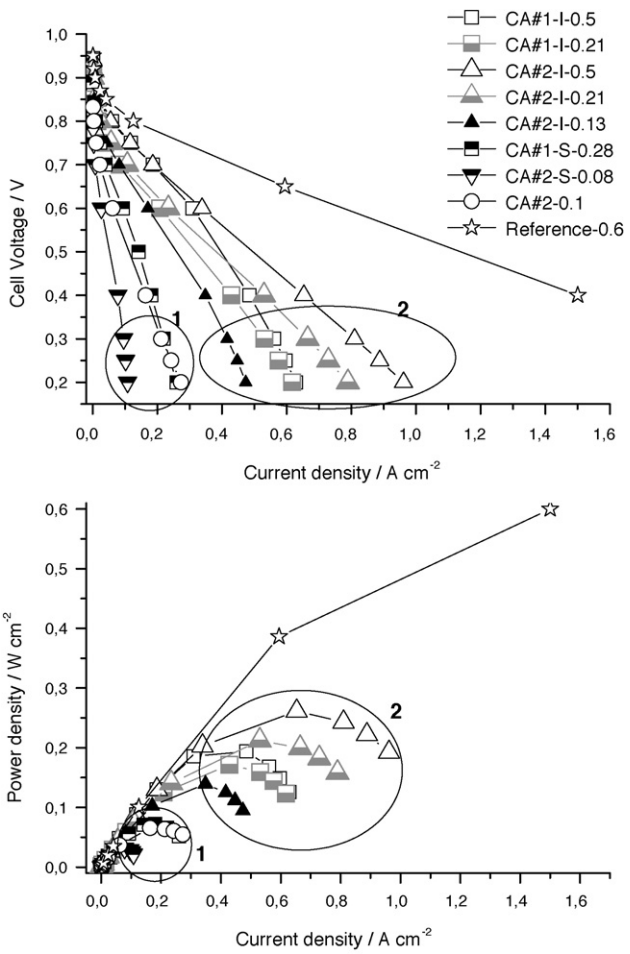

Fig. 4. Polarization curves (top) and power density (bottom). Comparison of the performance of the various carbon aerogel MEAs. $50\,cm^2$ single cells operated at 70 °C, P_{tot} H_2/air = 1.3/1.3 bar, stoichiometry H_2/air = 2/2.5 with fully humidified gas (R_H = 100%), stoichiometric flows when current density is higher than $0.24\,A\,cm^{-2}$ and constant flows for inferior current density.

Comparing the MEAs CA#1-I-0.5 and CA#2-I-0.5 in terms of power density in Fig. 4 exhibits that changing the nanostructure of the carbon aerogel has a major effect on the maximum power of the cells: 40% more power is drawn from CA#2-I-0.5 than CA#1-I-0.5 ($0.18\,W\,cm^{-2}$ vs. $0.25\,W\,cm^{-2}$). It is a first indication of the strong influence of the carbon aerogel nanostructure (and thus the catalytic layer nanostructure) on the cell performance at high current density. Since the Pt electrocatalytic properties are identical on both carbon aerogels, the polarization curves must differ in terms of ohmic resistance or transport properties. At this point, it is not possible to say which one of these parameters is the most significant one. It will be the purpose of the following part aiming at separating the kinetic, ohmic and transport limitations of the cell polarization.

Concerning CA#1-I-0.5 and CA#1-I-0.21 polarization curves, the same question arises to understand which limitation makes that the higher loading MEA (CA#1-I-0.5) intersects with the CA#1-I-0.21

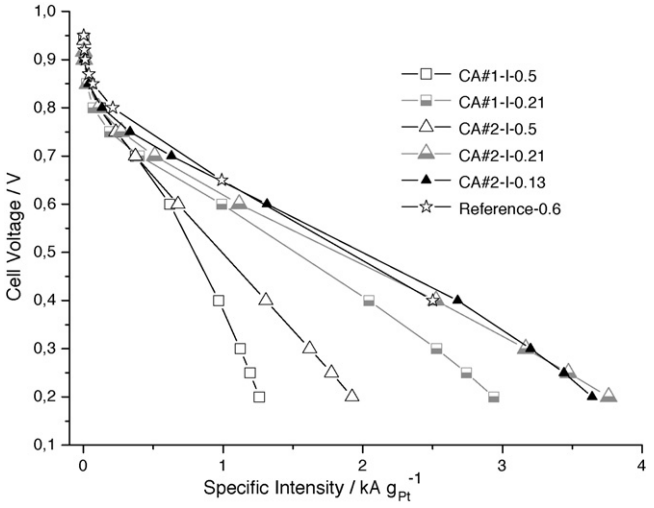

Fig. 5. Specific intensity polarization curves. Comparison of the carbon aerogel "ink MEAs". 50 cm^2 single cells operated at 70 °C, P_{tot} H_2/air = 1.3/1.3 bar, stoichiometry H_2/air = 2/2.5 with fully humidified gas (R_H = 100%), stoichiometric flows when current density is higher than 0.24 A cm^{-2} and constant flows for inferior current density.

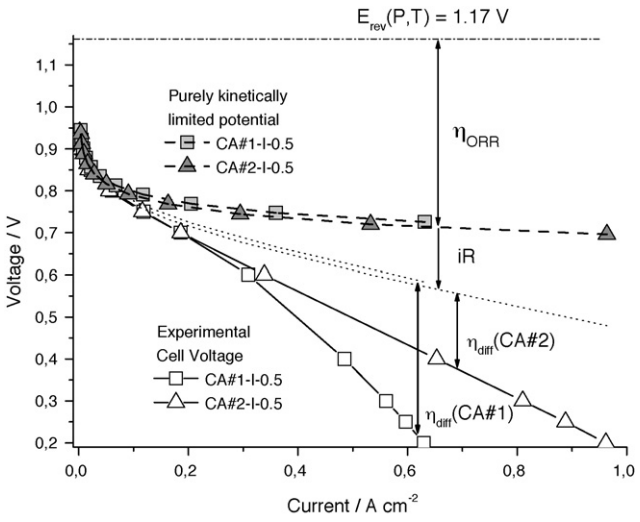

Fig. 6. Illustration of the voltage losses decomposition. Separation of ohmic and kinetic losses for CA#1-I-0.5 and CA#2-I-0.5 MEAs in order to obtain the mass-transport loss $\eta_{diff}(i)$. 50 cm^2 single cells operated at 70 °C, P_{tot} H_2/air = 1.3/1.3 bar, stoichiometry H_2/air = 2/2.5 with fully humidified gas (R_H = 100%), stoichiometric flows when current density is higher than 0.24 A cm^{-2} and constant flows for inferior current density.

polarization curve at high current density. We can only suppose that higher loading implies higher ohmic resistance or higher transport losses (because of higher thickness of the catalytic layer) without being able to distinguish between those two causes.

The loss of efficiency with the increase in Pt loading for a given carbon aerogel is clearly seen on the Pt-specific intensity polarization curves shown in Fig. 5. The MEAs with higher Pt-loading at the cathode (0.5 mg$_{Pt}$ cm^{-2}) exhibit lower Pt-specific performance. In fact, it is quite commonly observed that the Pt-specific performance does not increase with the platinum loading of the cathode [30]. Indeed, the higher the loading, the thicker the catalytic layer and the more critical it is to achieve a compromise between proton transport losses and mass transport losses (at high current densities). This compromise is less critical at low Pt-loading as reactants are transported over shorter distances. This explains why the low-loading MEA CA#2-I-0.13, and to a lesser extend CA#1-I-0.2 and CA#2-I-0.21 reach similar Pt-specific performance than the Reference-0.6 MEA which has the only commercially optimized cathode structure.

3.6. Voltage losses decomposition

In order to evaluate the contribution of the mass transport voltage losses to the polarization curves, we used an approach introduced by Gasteiger et al. [2], which is based on a the following decomposition of the cell voltage $E_{cell}(i)$:

$$E_{cell}(i) = E_{rev}(p_{H_2}, p_{O_2}, T_{cell}) - iR_{\Omega} - \eta_{ORR}(i) - \eta_{diff}(i) \quad (6)$$

with $\eta_{ORR}(i)$ the purely kinetic loss due to oxygen reduction reaction, R_{Ω} the ohmic resistance, $\eta_{diff}(i)$ the transport voltage loss and E_{rev} the reversible potential equals to 1.17 V in our experimental conditions (P = 1.3 bar, T = 70 °C, RH = 100%).

The process that we used to calculate $\eta_{diff}(i)$, is depicted in Fig. 6.

- The ohmic resistance R_{Ω} is firstly determined by a technique that will be explained in Section 3.6.1.
- The purely kinetically limited polarization curve (dashed line) can then be drawn from the fitting at low current density of the experimental polarization curve added of the ohmic loss iR_{Ω} (i.e. resistance-free polarization curve). The determination of these curves is detailed in Section 3.6.2. As given in Eq. (7), this polarization curve includes the 2 terms $\eta_{ORR}(i)$ and E_{rev}.
- Next, the ohmic loss iR_{Ω} is subtracted to the dashed line to obtain a polarization curve (dotted line) taking into account of 3 contributions $\eta_{ORR}(i)$, E_{rev} and iR_{Ω}. This curve differs with the experimental curve (plain line) only by the transport loss voltage loss $\eta_{diff}(i)$ as given in Eq. (6). This term is therefore calculated as the difference between the dotted line curve and the plain line curve.

3.6.1. High frequency MEA ohmic resistance

The determination of the ohmic resistance of the MEA was obtained from the measurement of the complex impedance $Z(\omega)$ shown in Fig. 7 at three cell voltages.

We can notice that the measured complex impedances of the various MEAs differ a lot but it is beyond the scope of this work to enter into the details of these plots. We only extract from these graphs the MEA ohmic resistance taken as the intersection with the real axis (see bottom graphs in Fig. 7) of the Nyquist plots at high-frequency (ca. 1.8 kHz).

The NE1035 membrane ohmic resistance which is included in the MEA high frequency ohmic resistance was estimated from the literature. Its value was calculated by taking the value of the N112 Nafion membrane fully humidified at 80 °C, 0.18 S cm^{-1} [2] and corrected by their difference in thickness, assuming that the differences in elaboration processes between N112 and NE1035 induce an increase of 10% in the proton conductivity.

The comparison of the high frequency ohmic resistance of the MEAs in Table 5 suggests two observations. Firstly, the MEAs prepared with CA#1 and CA#2 carbon aerogels have similar MEA resistances. Secondly, for both carbon aerogels structures, a reduction of the platinum loading from 0.5 to 0.21 mg$_{Pt}$ cm^{-2} yields only a small decrease of the MEA resistance (~10% reduction). Thus the thickness of the catalytic layer has not a strong effect on the MEA ohmic resistance. This means that the bulk resistivity of the carbon aerogel layer is not significant compared with the contact resistances of the catalytic layer with the membrane on one side and with the GDL on the other side.

The relatively large difference between the resistances of the Reference-0.6 MEA and the carbon aerogel MEAs must certainly

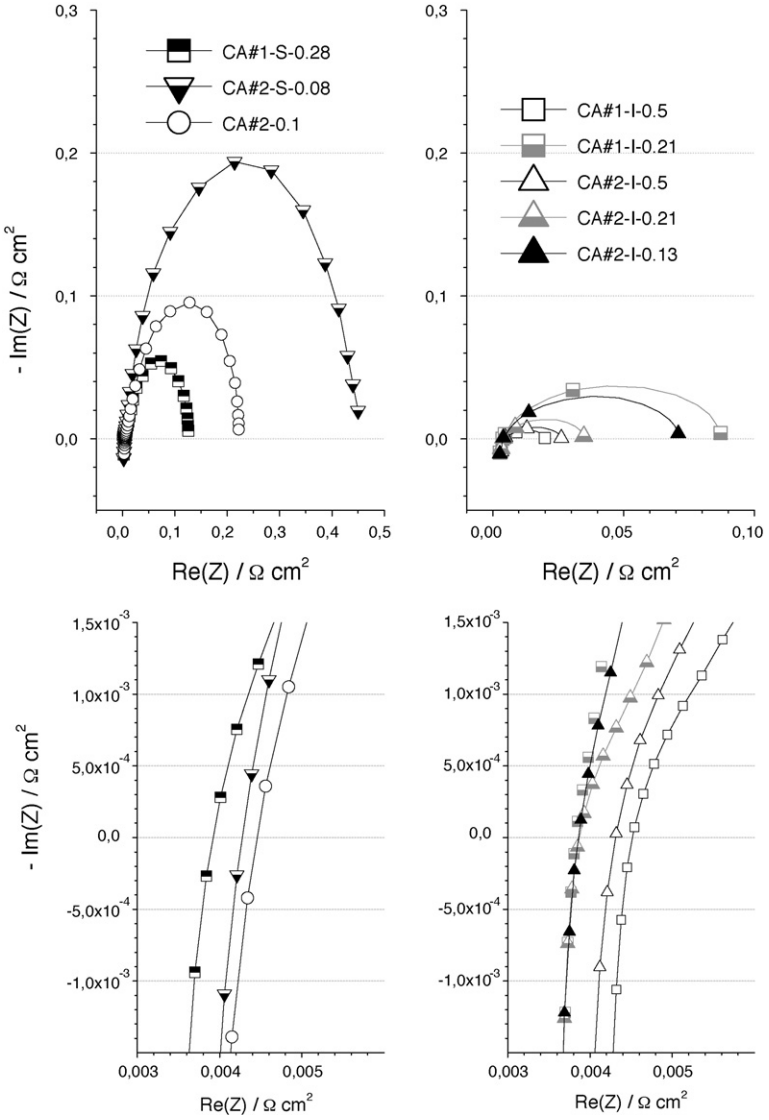

Fig. 7. Nyquist plots of the carbon aerogel MEAs. Impedance $Z(\omega)$ measured at cell voltage = 0.8 V. 50 cm^2 single cells operated at 70 °C, P_{tot} H_2/air = 1.3/1.3 bar, stoichiometry H_2/air = 2/2.5 with fully humidified gas (R_H = 100%), stoichiometric flows when current density is higher than 0.24 A cm^{-2} and constant flows for inferior current density.

originate in these contact resistances. At least the contact resistance between the GDL and the catalytic layer would certainly require be optimized by employing a carbon aerogel/PTFE intercalation layer instead of carbon black/PTFE.

We can also notice in Table 5, that the MEA ohmic resistances taken at different voltages decrease when the cell voltage is higher (from 0.4 V to OCV). Actually this is a tendency observed in the literature [21]. It is explained by the fact that as the cell voltage decreases, the current intensity increases meaning higher proton flow from the anode to the cathode. As this flow increases, it drags more water molecules from anode side to cathode side, yielding a partial drying of the membrane at the anode side, which thus becomes more resistive.

In conclusion, these measurements show that neither the structure of the carbon aerogel nor the layer thickness have a significant influence on the high-frequency resistance of the MEAs.

Table 5
Comparison of the high-frequency ohmic resistance of the MEAs at 3 cell voltages (OCV, 0.8 and 0.4 V). The membrane resistance is calculated from literature data.

	R_{HF} at 0.4 V (Ω cm^{-2})	R_{HF} at 0.8 V (Ω cm^{-2})	R_{HF} at OCV (Ω cm^{-2})
CA#1-I-0.5	0.246	0.225	0.202
CA#1-I-0.21	0.198	0.191	0.19
CA#2-I-0.5	0.248	0.213	0.223
CA#2-I-0.21	0.195	0.187	0.175
N1035	0.05	0.05	0.05
Reference-0.6	0.165	0.142	0.141

3.6.2. Kinetic loss (η_{ORR})

3.6.2.1. Tafel slope. It has been shown by Gasteiger et al. [2] that the resistance-free polarization curve (i.e. cell voltage added of iR_Ω) of carbon black-based, state of the art MEA, operated under H_2/O_2 was solely determined by the ORR kinetic and E_{rev} as given in the following equation:

$$E^{H_2/O_2}_{iR\text{-free}}(i) = E_{rev}(p_{H_2}, p_{O_2}, T_{cell}) - \eta_{ORR}(i) \quad (7)$$

They also showed that the kinetic loss η_{ORR} followed a Tafel behavior at low current density as given in the following equation:

$$\eta_{ORR}(i) \propto b \log(i_{eff}) \quad (8)$$

where $i_{eff} = i - i_x$, i_x being the H_2-cross-over current density due to H_2 permeability across the Nafion membrane and b the Tafel slope.

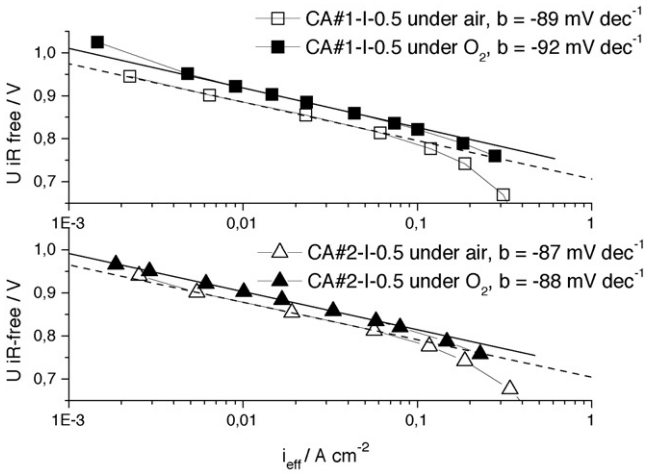

Fig. 8. Polarization curves of carbon aerogel MEAs under air and O_2. Comparison of the low current density voltage losses. Resistance corrected cell voltage (iR-free). 50 cm^2 single cells operated at 70 °C, P_{tot} H_2/air = 1.3/1.3 bar. The stoichiometry of flow rates H_2/air = 2/2.5 (stoichiometry H_2/O_2 = 2/9) with fully humidified gas (R_H = 100%), stoichiometric flows when current density is higher than 0.24 A cm^{-2} and constant flows for inferior current density, b = Tafel slopes.

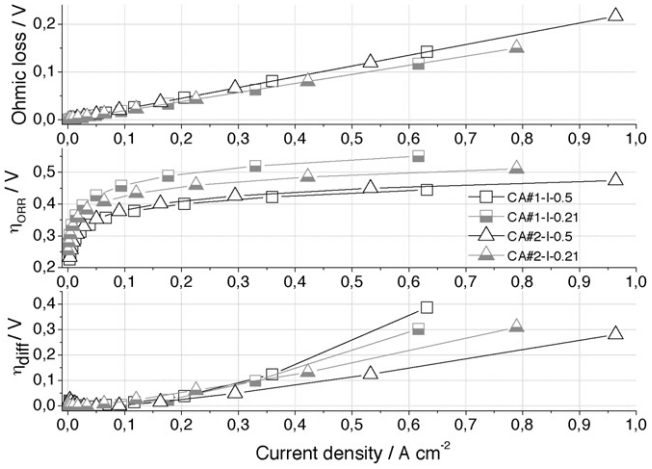

Fig. 9. Voltage losses of carbon aerogel MEAs: ohmic loss, ORR kinetic loss η_{ORR} and mass-transport loss η_{diff}. Comparison of the "ink" MEAs made with CA#1 and CA#2 and with two platinum loadings. 50 cm^2 single cells operated at 70 °C, P_{tot} H_2/air = 1.3/1.3 bar, stoichiometry H_2/air = 2/2.5 with fully humidified gas (R_H = 100%), stoichiometric flows when current density is higher than 0.24 A cm^{-2} and constant flows for inferior current density.

We thus measured the polarization curves of CA#1-I-0.5 and CA#2-I-0.5 MEAs using O_2 at the cathode and compared it to the air performance. In Fig. 8, the iR-free polarization curves are drawn.

Similar Tafel slopes are measured for O_2 and air at low current density for both MEAs (CA#1 and CA#2) which is in agreement with the theoretical reaction order to O_2 partial pressure equals to one [31]. The offsets between the air and O_2 polarization curves (25 and 32 mV for CA#1 and CA#2, respectively) are due to the difference in O_2 partial pressure. These values are close to the theoretical potential offset due to the reversible potential equals to 29 mV.

The obtained values of Tafel slopes are in the same range (-90 ± 3 mV dec^{-1}) than MEAs made with E-TEK catalysts at the cathode and measured in similar configurations [32]. State-of-the-art platinum-supported catalysts (TKK) with state-of-the-art MEA components exhibit higher kinetic activity with Tafel slopes of -74 ± 4 mV dec^{-1} [2]. One of the reasons for the relatively low Tafel slopes that we measured on Pt/CA could be due to the high carbon surface area. Indeed, the carbon aerogel high surface area could contribute to the ORR yielding a decrease in the Tafel slope as the mechanism of reduction of oxygen on carbon implicates only 2 electrons (mechanism yielding hydrogen peroxide) rather than 4 on platinum.

3.6.2.2. H_2/O_2 electrocatalytic activities of the cathodes in MEA configuration at 0.9 V. From the measured polarization curves under O_2, the electrocatalytic activities of the Pt/CAs are compared in Table 6 with literature data normalized at 1 bar.

The data in Table 6 underline that the mass activities i_m at 0.9 V of the Pt/CAs-based cathodes are relatively similar ($20 - 30$ A g_{Pt}^{-1}) for both carbon aerogels CA#1 and CA#2 and both MEA Pt-loadings. Compared with the literature data, the electrocatalytic activities of the carbon aerogel-based cathodes differ mostly in terms of mass activity. This mainly originates from their lower Pt utilization ratio which is thus a critical point to be optimized in our MEAs. This will be done in future works by optimizing the inks and the MEA elaboration processes [24].

3.6.2.3. H_2/air cathodes mass-transport losses determination (η_{diff}): comparison of two carbon aerogels structure and two platinum loadings. We show in Fig. 9 the result of the decomposition of the polarization curves as three cell voltage losses $\eta_{diff}(i)$, $\eta_{ORR}(i)$ and the ohmic loss for 4 "ink" MEAs.

The first feature appearing when comparing these voltage losses is that $\eta_{ORR}(i)$ is the most important one at low current density ($i < 0.1$ A cm^{-2}). As current density increases, $\eta_{diff}(i)$ becomes the most important part of the decrease in the cell voltage. Between 0.1 and the maximum current density of the MEAs, the increase of $\eta_{ORR}(i)$ is less than 100 mV, iR_Ω amounts to 200 mV whereas the one of $\eta_{diff}(i)$ is at least 300 mV. Clearly at high current density, mass-transport loss $\eta_{diff}(i)$ becomes a major contribution to the cell polarization.

Concerning the comparison between the two carbon aerogels CA#1 and CA#2, the graphs of the kinetic and ohmic losses confirm that they are not influenced by the nanostructure of the carbon aerogel whereas $\eta_{diff}(i)$ of CA#1 and CA#2 differ to a great extent. It is the mass-transport losses which differentiate the most the performance of the MEAs. The mass-transport losses of the CA#2 MEAs are significantly lower than the ones made with CA#1 at both Pt loadings. At 0.6 A cm^{-2}, the mass-transport loss of CA#2-I-0.5

Table 6
Electrocatalytic activities at 0.9 V vs. NHE of two carbon aerogel-based cathodes operated with oxygen from the iR-free performance shown in Fig. 8. Comparison with two carbon black-based cathodes.

	L_{Pt} (mg_{Pt} cm^{-2}) ±10%	S_{Pt}(m^2_{Pt} g^{-1}_{Pt})	b (mV dec^{-1})	i (mA cm^{-2})	i_m(A g^{-1}_{Pt}) ± 10%	i_s(μA cm^{-2}_{Pt}) ± 10%
CA#1-I-0.5	0.5	17.1	−89	14.8	30	173
CA#1-I-0.21	0.21	20.7	−110	4.2	20	97
CA#2-I-0.5	0.5	15.7	−87	10.4	21	132
CA#2-I-0.21	0.21	26	−93	4.7	22	86
CA#2-I-0.13	0.13	21	−98	3.5	27	132
Pt/Vu ETEK (40 Pt wt.%) [32]	0.38	32	−90	24	64	200
Pt/Vu TKK (50 Pt wt.%) [33]	0.25	62	NA	17	70	110

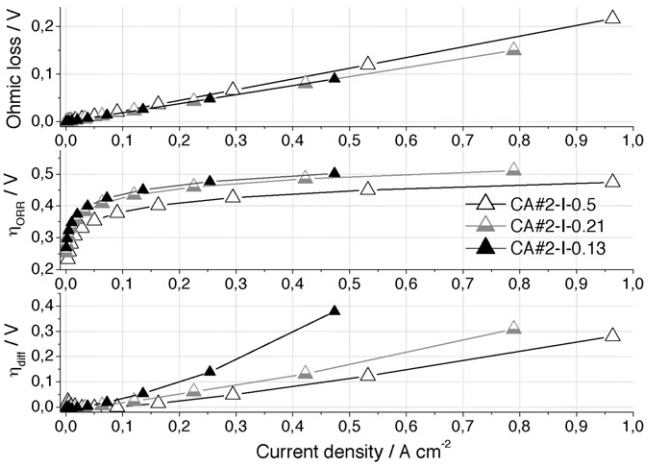

Fig. 10. Voltage losses of carbon aerogel CA#2 MEAs. Comparison of three cathodes platinum loadings. 50 cm^2 single cells operated at 70 °C, P_{tot} H_2/air = 1.3/1.3 bar, stoichiometry H_2/air = 2/2.5 with fully humidified gas (R_H = 100%), stoichiometric flows when current density is higher than 0.24 A cm^{-2} and constant flows for inferior current density.

amounts to 145 mV vs. almost the double for CA#1-I-0.21 (286 mV) and even more for CA#1-I-0.5 (360 mV).

Thus, first relations between the nanostructure of the carbon aerogel-based catalytic layers and their performance can be drawn. The carbon aerogel CA#2 with, in the beginning, smaller pore-size and porous volume but which constituted more porous catalytic layers than CA#1, yields higher performance at high current density. In other words, we measured that the higher the porosity of the catalytic layer (in the mesopores domain), the lower its mass-transport limitation. This measurement means that the transport of protons in the mesopores of the catalytic layer is not limiting compared with the oxygen transport. Indeed, if proton transport was limiting, MEAs made with carbon aerogel CA#1 having initially larger pores but finally more filled with Nafion would be less limited than CA#2 MEAs.

It should be recalled that in our previous study using a half-cell configuration to compare the Pt/CAs [10], CA#1 MEAs performed better than CA#2 MEAs at high current density. This is because, in this prior work, the catalytic layers were partially flooded with a liquid electrolyte (1 M H_2SO_4) as they were immersed in a glass electrochemical cell and O_2 diffusion is easier in Nafion than in aqueous acid solution [33–36]. So both experimental results obtained with the two different configurations (fuel cell and half-cell testing) can be interpreted by taking into account that O_2 transport and not proton transport is the most discriminating phenomenon in both cases. To summarize, in the free gas-pores situation (fuel-cell testing), the higher the porosity, the easier the O_2-diffusion whereas, in the case of flooded pores, the higher the quantity of Nafion in the pores, the easier the O_2 diffusion and the higher the fuel cell output current.

Finally concerning the comparison between the different Pt loadings of the MEAs, the CA#1 and CA#2 MEAs behaves differently: $\eta_{diff}(i)$ of CA#1-I-0.5 is higher than CA#1-I-0.21 which seems logical as thicker layer (higher Pt-loading) should induce higher transport limitation. But the opposite trend is measured for CA#2:CA#2-I-0.21, exhibits significantly higher mass-transport losses than CA#2-I-0.5. This result is confirmed by the MEA CA#2-I-0.13 presented in Fig. 10. The CA#2-I-0.13 cathode exhibits about the same kinetic properties than the other cathodes but its mass-transport overpotential is much higher than the other MEAs. This particular result was in fact already observed by Gasteiger et al. [2] on state-of-the-art MEAs based on cathode containing Pt/carbon black catalyst.

We can propose an interpretation to this phenomenon, as follows. The porosities of the lower loading catalytic layers which are thinner are more intruded by the softened Nafion during the hot-pressing step. Their porosity would thus be much more (in proportion) filled of Nafion than the thicker layers yielding a more important mass-transport limitation in these layers. We will address this question in future works.

4. Conclusion

The two carbon aerogels synthesized for this study had high specific surface area because they are made of small primary carbon particles and high porous volume because they are synthesized by a sol–gel technique. They were differentiated by their pore-size distribution, adjusted by the synthesis parameters of the initial gels. So they were interesting Pt-support for studying the mass-transport losses in the cathode catalytic layer of H_2/air-fed PEM fuel cell. This was done by testing 50 cm^2 MEAs as single cells.

This experimental work gave the following results. Firstly, it was found that the higher the initial pore-size of the carbon aerogel, the lower the porosity of the resulting catalytic layer because of a more important penetration of Nafion into the larger pore-size carbon aerogel.

Secondly, the polarization curves of the MEAs were found to be highly influenced by the carbon aerogel nanostructure. The cell voltages of the MEAs were decomposed in three voltage losses: the kinetic loss $\eta_{ORR}(i)$, the ohmic resistance loss and the transport loss $\eta_{diff}(i)$. The transport loss was found to be significantly influenced by the carbon aerogels pore-size distribution whereas the two other terms were almost independent from it.

Thirdly, the transport loss comparison between the MEA made with the two different carbon aerogels showed that the higher the porosity of the catalytic layer, in the mesoporous range, the lower the mass-transport loss in fuel cell configuration.

And finally, comparing $\eta_{diff}(i)$ of MEAs with different Pt loadings showed that the lower the electrode Pt-loading, the higher the mass-transport limitation.

As a perspective we underline that to improve the performance of carbon aerogel cathodes, especially at low current density, an essential parameter that will have to be addressed in future work is the Nafion insertion in the micron sized grains of carbon aerogel. The Nafion insertion technique which was adapted from carbon black catalytic layers will certainly have to be adapted to the particular structure of the carbon aerogels. Last, even though the highly porous structure and nanoscale texture of the carbon aerogels renders difficult a perfect Nafion insertion in it, this feature may be interesting for the Pt stability over the time.

Acknowledgement

The authors are grateful for financial support from Renault Research Direction.

References

[1] M. Uchida, Y. Fukuoka, Y. Sugawara, H. Ohara, A. Ohta, J. Electrochem. Soc. 145 (11) (1998) 3708.
[2] H.A. Gasteiger, S.S. Kocha, B. Sompalli, F.T. Wagner, Appl. Catal. B 56 (1–2) (2005) 9.
[3] R.W. Pekala, J.C. Farmer, C.T. Alviso, T.D. Tran, S.T. Mayer, J.L. Miller, B. Dunn, J. Non-Cryst. Sol. 225 (1998) 74.
[4] H. Hirashima, C. Kojima, K. Kohama, H. Imai, V. Balek, H. Hamada, M. Inaba, J. Non-Cryst. Sol. 225 (1998) 153.
[5] M.V. Williams, H.R. Kunz, J.M. Fenton, J. Electrochem. Soc. 152 (3) (2005) A635.
[6] B. Kienitz, H. Baskaran, T. Zawoddzinski Jr., B. Pivovar, ECS Trans. 11 (1) (2007) 777.
[7] M.N. Tsampas, A. Pikos, S. Brosda, A. Katsounis, C.G. Vayenas, Electrochim. Acta 51 (13) (2006) 2743.
[8] C.G. Vayenas, M.N. Tsampas, A. Katsounis, Electrochim. Acta 52 (6) (2006) 2244.

[9] J. Marie, S. Berthon-Fabry, M. Chatenet, E. Chainet, N. Cornet, P. Achard, J. Appl. Electrochem. 37 (2007) 147.
[10] J. Marie, S. Berthon-Fabry, P. Achard, M. Chatenet, E. Chainet, N. Cornet, R. Pirard, ECS Trans. 1 (6) (2006) 509.
[11] J. Marie, S. Berthon-Fabry, P. Achard, M. Chatenet, A. Pradourat, E. Chainet, J. Non-Cryst. Sol. 350 (2004) 88.
[12] S.-J. Lee, T.L. Yu, H.-L. Lin, W.-H. Liu, C.-L. Lai, Polymer 45 (2004) 2853.
[13] M.S. Wilson, S. Gottesfeld, J. Appl. Electrochem. 22 (1992) 1.
[14] S. Lister, G. McLean, J. Power Sources 130 (2004) 61.
[15] G.W. Scherer, J. Non-Cryst. Sol. 225 (1998) 192.
[16] R. Pirard, C. Alié, J.-P. Pirard, in: S. Sakka, R.M. Almeida (Eds.), Handbook of Sol–Gel Science and Technology, vol. 2. Characterization of Sol–Gel Materials and Products, Kluwer Academic Publishers, London, 2005, p. 211.
[17] A. Kuver, I. Vogel, W. Vielstich, J. Power Sources 52 (1994) 77.
[18] G.C. Li, P.G. Pickup, Electrochim. Acta 49 (24) (2004) 4119.
[19] K. Kinoshita, Carbon-Electrochemical and Physicochemical Properties, J. Wiley and Sons–Wiley Interscience, New York, 1988, p. 297.
[20] M. Eikerling, A.A. Kornyshev, E. Lust, J. Electrochem. Soc. 152 (1) (2005) E24.
[21] K.R. Cooper, M. Smith, J. Power Sources 160 (2006) 1088.
[22] R. Makharia, M.F. Mathias, D.R. Baker, J. Electrochem. Soc. 152 (5) (2005) A970.
[23] J. Xie, F. Garzon, T. Zawodzinski, W. Smith, J. Electrochem. Soc. 151 (7) (2004) A1084.
[24] H. Xu, E. Brosha, F. Garzon, F. Uribe, M. Wilson, B. Pivovar, ECS Trans. 11 (1) (2007) 383.
[25] W.J. Liu, B.L. Wu, C.S. Cha, J. Electroanal. Chem. 476 (1999) 101.
[26] K. Shinozaki, T. Hatanaka, Y. Morimoto, ECS Trans. 11 (1) (2007) 497.
[27] B. Fang, Y.-Z. Wei, K. Maruyama, M. Kumagai, J. Appl. Electrochem. 35 (2005) 229.
[28] P. Stonehart, P. Ross, Electrochim. Acta 21 (6) (1976) 441.
[29] F. Gloaguen, R. Durand, J. Appl. Electrochem. 27 (1997) 1029.
[30] Z. Qi, A. Kaufman, J. Power Sources 113 (2003) 37.
[31] O. Antoine, Y. Bultel, R. Durand, J. Electroanal. Chem. 499 (2001) 85.
[32] H.A. Gasteiger, W. Gu, R. Makharia, M.F. Mathias, B. Sompalli, in: W. Vielstich, A. Lamm, H.A. Gasteiger (Eds.), Handbook of Fuel Cells, vol. 3. Fundamentals, Technology and Applications, Wiley, Chichester, 2003, p. 593.
[33] S.S. Kocha, in: W. Vielstich, A. Lamm, H.A. Gasteiger (Eds.), Handbook of Fuel Cells, vol. 3. Fundamentals, Technology and Applications, Wiley, Chichester, 2003, p. 538.
[34] A.T. Haug, R.E. White, J. Electrochem. Soc. 147 (3) (2000) 980.
[35] V.I. Basura, P.D. Beattie, S. Holdcroft, J. Electroanal. Chem. 458 (1998) 1.
[36] K. Kinoshita, Electrochemical Oxygen Technology, J. Wiley and Sons, Wiley Interscience, New York, 1992, p. 4.